OPEN

NPG Asia Materials (2015) 7, e154; doi:10.1038/am.2014.124

www.nature.com/am

ORIGINAL ARTICLE

Observation of a giant two-dimensional band-piezoelectric effect on biaxial-strained graphene

Xiaomu Wang[1,2,4,5], He Tian[1,4], Weiguang Xie[2,3,4], Yi Shu[1], Wen-Tian Mi[1], Mohammad Ali Mohammad[1], Qian-Yi Xie[1], Yi Yang[1], Jian-Bin Xu[2] and Tian-Ling Ren[1]

Piezoelectric materials used in the development of nanoscale mechanical sensors, actuators and energy harvesters have received much attention. More recently, devices made of graphene are of particular interest because of graphene's intriguing electronic and mechanical properties. Intrinsic graphene has long been considered devoid of the piezoelectric effect, although flexoelectricity has been exploited to demonstrate piezoelectricity in functionalized graphene and graphene nanoribbons. The perceived lack of this property has restricted graphene's use in nanoelectromechanical systems (NEMS) for electromechanical coupling purposes. Here an unprecedented two-dimensional (2D) piezoelectric effect on a strained/unstrained graphene junction is reported. In stark contrast to the bulk piezoelectric effect that results from the occurrence of electric dipole moments in solids, the 2D piezoelectric effect arises from the charge transfer along a work function gradient introduced by the biaxial-strain-engineered band structure. The observed effect, termed the band-piezoelectric effect, exhibits an enormous magnitude due to the ultrathin structure of graphene. On the basis of the band-piezoelectric effect, a graphene nanogenerator and a pressure gauge were fabricated. The results not only provide a versatile NEMS platform for sensing, actuating and energy harvesting, but also pave the way for efficiently modulating graphene via strain engineering.
NPG Asia Materials (2015) **7,** e154; doi:10.1038/am.2014.124; published online 16 January 2015

INTRODUCTION

Graphene has proven to be a remarkable material for nanoscale devices because of its unique physical properties.[1] In particular, graphene exhibits striking mechanical stiffness (with 1 TPa Young's modulus), ultrathin structure (down to a single atomic layer) and exceptional robustness (stretchable up to 20%), which make it an ideal platform for NEMS.[2–8] In the context of NEMS, electromechanical coupling is an important and highly desirable property. Among the various coupling methods, the piezoelectric effect, in which a material becomes electrically polarized under external strain, is the most popular method. The piezoelectric effect is frequently used for dynamical control of NEMS devices in sensing, actuating and transducing applications.[9–14] Unfortunately, all of the traditional piezoelectric mechanisms are not applicable to intrinsic graphene. Because of the centrosymmetric nature of graphene, the piezoelectric effect is absent in intrinsic graphene.[15] Achievement of piezoelectricity in previous pioneering works requires the functionalization or nanopatterning of graphene to break this centrosymmetry.[16,17] Furthermore, in its intrinsic (semi-)metallic states, graphene is clearly non-piezoelectric and/or non-flexoelectric.[17] In addition, its single-atom thickness leads to an ill-defined out-of plane strain gradient and a questionable breakage of the centrosymmetric flexoeletricity. Therefore, the flexoelectricity is in fact limited despite the expectation of its enhancement in nanoscale systems.[18,19] In summary, although 2D piezoelectricity has been demonstrated for functionalized graphene and graphene nanoribbons, intrinsic graphene has long been considered devoid of the piezoelectric effect, which could provide a solid electromechanical coupling pathway. Nevertheless, strain engineering or using a pseudo-magnetic field is a predicted means of opening a bandgap in intrinsic graphene.[20,21] Although a series of spectroscopic works have previously reported the strain-modified graphene electronic structure, the direct electromechanical coupling of graphene under shear strain has not yet been demonstrated.[22–26]

In this article, a unique 2D piezoelectric effect on a biaxial-strained graphene/pristine graphene junction-based NEMS system is demonstrated. An in-plane biaxial strain-controlled electrical polarization across the junction can be achieved using this effect. The observed piezoelectric effect, which is attributed to a strain-modified band structure, is termed the band-piezoelectric effect. *In situ* Kelvin probe force microscopy and transport measurements were used to monitor the spatial distribution of the quasi-Fermi levels and to provide evidence of bandgap opening. Furthermore, the band-piezoelectric effect enabled the fabrication of a novel piezoelectric nanogenerator and a high-sensitivity piezoresistive pressure sensor.

[1]Institute of Microelectronics and Tsinghua National Laboratory for Information Science and Technology (TNList), Tsinghua University, Beijing, China; [2]Department of Electronic Engineering, The Chinese University of Hong Kong, Hong Kong, SAR, China and [3]Siyuan Lab, Department of Physics, Jinan University, Guangzhou, China
[4]These authors contributed equally to this work.
[5]Current address: Department of Electrical Engineering, Yale University, New Haven, CT 06511, USA.
Correspondence: Professor T Ren or Professor J-B Xu, Tsinghua National Laboratory for Information Science and Technology (TNList), Institute of Microelectronics, Tsinghua University, Beijing 100084, China.
E-mail: RenTL@tsinghua.edu.cn or jbxu@ee.cuhk.edu.hk
Received 9 September 2014; revised 11 November 2014; accepted 17 November 2014

MATERIALS AND METHODS

Fabrication of 2D graphene NEMS

The device structure is schematically shown in Figure 1a. The device fabrication was conducted on a highly p-doped silicon wafer with a 300-nm thick thermally grown SiO_2 dielectric layer. Silica cavities with a 5-μm diameter were patterned using photolithography and then etched 400-nm deep via a reactive-ion etching process at 2 Pa under Ar atmosphere and 20 s.c.c.m. CF_4 flow using a 50 W of radio frequency power (Supplementary Figure S1). Subsequently, few-layer graphene (mostly mono- and bilayer samples were used in our study) were prepared by mechanical exfoliation of Kish graphite.[27] Gold electrodes were cut out from a foil, lifted with a tip and then electrically connected to suspended graphene (as schematically shown in Figure 1b) in a 'loosely clamped' configuration to avoid electrode-induced strain.[28] Note that there are two challenges in the fabrication process. First, the sealed cavity prevents traditional patterning methods, such as lithography, because solution treatment always causes the suspended graphene to collapse (see Supplementary Information for details). In our experiments, a 'lithography-free' method was used to fabricate the electrodes, as previously reported by Wang *et al.*[29] Second, graphene samples should be carefully selected to maximize the strain and to obtain controllable deformation. For these purposes, membranes that exactly match the cavity width are required, such as those shown in Figures 1c and d. Samples with a large supported part or partially covered cavity should be avoided. Furthermore, the initial internal stress in graphene devices must be examined in advance.[30] In fact, we observed large intrinsic ripples that reduce the pressure load in some samples (Supplementary Figure S3).

Nanoindentation of 2D graphene NEMS

The nanoindentation experiments were performed using an atomic force microscope (AFM; Bruker Dimension ICON, Billerica, MA, USA) under contact mode. For piezoresistive and piezoelectric measurements, non-conductive silicon tips and silicon tips with TiN-conductive coating layers were used, respectively. The spring constants of all the tips were ~ 3 N m^{-1}. In the piezoresistive experiment, the scan range was initially set to 6 μm (with direction from edge to center) to fully deflect the graphene membrane. The load was then moved to the center of the membrane by gradually decreasing the scan range to 100 nm, which ensured a constant deformation (strain). In the piezoelectric measurements, the scan range and scan rate were kept at 3 μm and 1.6 Hz, respectively. The electric measurements were performed using a semiconductor analyzer (Keithley 4200, Keithley Instruments Inc., Cleveland, OH, USA) with pre-amplifiers.

RESULTS

Piezoelectric effects in suspended graphene membrane

The band-piezoelectric effect in this NEMS platform is first demonstrated by studying the spatial surface potential (SP) distribution in bent graphene. To achieve this, Kelvin probe force microscopy was used to obtain an *in situ* map of the Fermi levels of deformed graphene. In this scenario, a back-gate voltage is applied to bend the graphene while the deformation and work functions were simultaneously measured using an AFM in a dual-pass scan mode. The

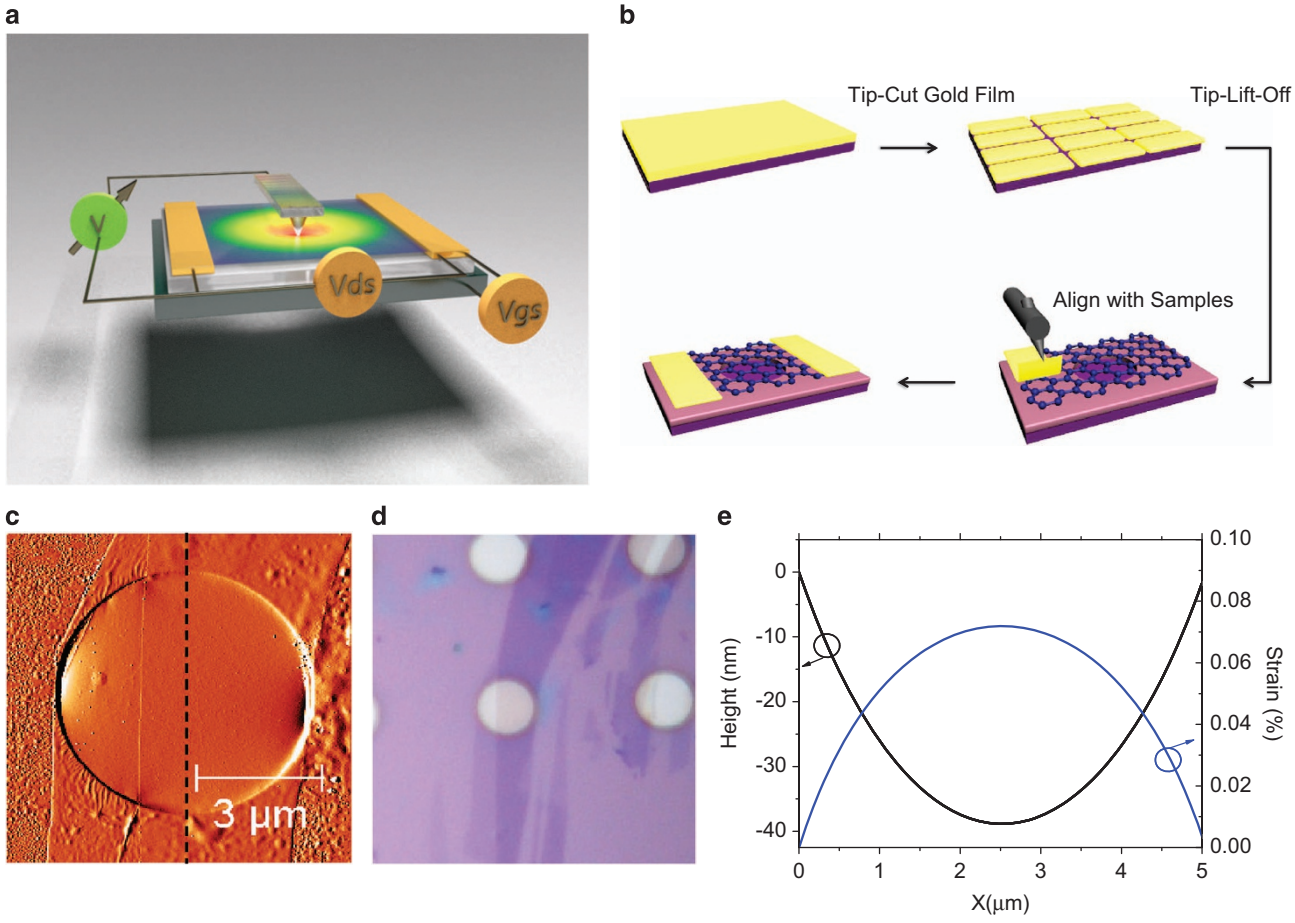

Figure 1 Suspended graphene membrane NEMS. (**a**) Schematic of the suspended graphene membrane cavity and the nanoindentation measurement setup. As a result of the AFM tip indenting the graphene membrane, the charge gradient in this membrane is expressed by a color change. (**b**) The lithography-free process flow. (**c**) AFM and (**d**) optical microscope images of a typical sample containing a monolayer graphene channel. (**e**) FEM simulation of the suspended graphene membrane pressed by an AFM tip with a set point of 80 nm. AFM, atomic force microscope; NEMS, nanoelectromechanical systems.

deformation and SP of the graphene membrane under different gate voltages are shown in Figures 2a and b (device #1). Here to better study the pressure-induced modification of suspended graphene, we focus on the SP differences between the suspended and supported graphene. Therefore, the global SP shifts in response to different gate voltages are removed from the curves in Figure 2b. For a small gate voltage, the graphene membrane is nearly unchanged, with only a small natural bending. Because the dielectric capacitance density is different for the supported and suspended graphene parts (C_{Silica}:C_{air} = 5.2:1), the Fermi level in the suspended membrane is higher than the Fermi level outside the cavity. Under a − 1 V gate voltage, the measured SP difference (~30 meV) approximately agrees with the theoretical Fermi-level shift (21 meV). With increasing gate voltages, the enhanced capacitive force bends the graphene down. However, the Fermi level of the bent graphene becomes continuously lower compared with that of the supported graphene, which is in stark contrast to the theoretical results that only consider different electrical doping levels arising from the dissimilar dielectrics. Under a gate voltage of − 4 V, the measured Fermi level in the center is ~ 120 meV lower than the supported part. By contrast, the electrical gating effect predicts that the Fermi level at the center should be 80 meV higher. This anomalous electric doping effect indicates that the biaxial strain modifies the electronic structure of graphene and introduces a potential gradient across the cavity boundary. Consequently, this potential difference drives charges separately in the bent interface, resulting in piezoelectric behavior.

The band-piezoelectric effect is further demonstrated by anomalous gate-controlled deformation. Under large gate voltages, the graphene membrane exhibits anomalous up-bending that is opposite to the capacitive force interaction resulting from electrical gating, as illustrated in Figures 2c–e (device #2). (The ripples in the AFM curves were attributed to tip-induced resonance. See Supplementary Information for details.) Interestingly, the up-bending behavior exhibits different characteristics for different gate voltage polarities. Under a positive gate voltage (n-type doping of graphene), the membrane bends upward immediately on applying a voltage above a certain threshold (Figure 2c). This phenomenon can be understood

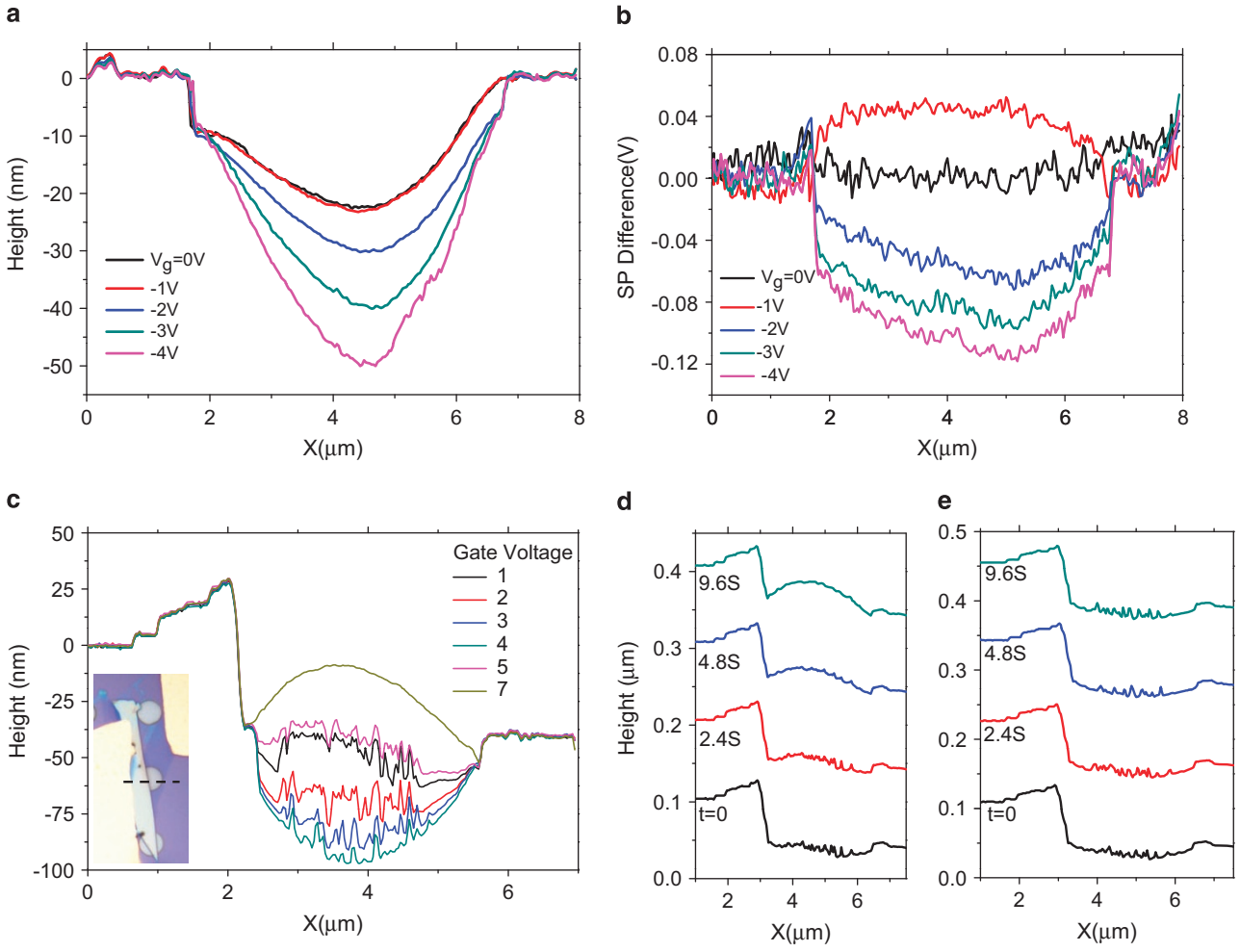

Figure 2 Piezoelectric effect of graphene NEMS revealed by KPFM measurements. (**a**) Mechanical deformation of the suspended graphene membrane under different negative back-gate voltages. (**b**) Surface potential difference distribution of the bent membrane in **a**. The scan line follows the dashed line in Figure 1c. (**c**) Anomalous mechanical deformation of the suspended graphene membrane under different positive gate voltages. Up-bending is observed for large gate voltages. The scan line follows the dashed line in the inset. The edges between (monolayer) suspended graphene, graphite and the supported part are marked with dashed lines. Inset: Optical image of the device in panel **c**. (**d**) Temporal evolution of the mechanical deformation of the device under − 5 V gate voltage scanned by an AFM tip biased at − 1 V and (**e**) AFM tip biased at 1 V. AFM, atomic force microscope; KPFM, Kelvin probe force microscopy; NEMS, nanoelectromechanical systems.

by considering the reversed polarity between electrical dopants and piezoelectric charges, that is, the interaction turns to a repulsive Coulomb interaction when the piezoelectric charges dominate. However, in the case of a negative gate voltage (p-type doping of graphene), the membrane only bends upward after scanning it with a negatively biased AFM tip. Furthermore, the membrane bends upward gradually, and the entire process typically takes a few tens of seconds to complete (Figure 2d). The deformation is otherwise unaltered, excluding the possible contribution from electrostatic interactions between the graphene membrane and the AFM tip (Figure 2e). Scanning the graphene membrane by a negatively biased tip under tapping mode, the positive charges are gradually removed from the graphene, giving rise to a converse piezoelectric effect, which may explain the anomalous up-bending under negative gate voltages. To verify the biaxial-strain-engineered graphene band alternation, we fabricated a microcavity and covered it with a graphene membrane. This membrane was deformed by nanoindentation and the resulting transport properties were measured.

DISCUSSION

Biaxial strain-modified graphene band structure

To explore the mechanism of our 2D band-piezoelectric effect, it is necessary to understand how the biaxial strain affects the electronic properties of graphene. A useful tool to understand this influence is the study of the dynamical transport of graphene field-effect transistor during bending of the suspended membrane. The measurement was performed while the suspended membrane was pressed by an AFM tip. The deformation and corresponding transport results under different pressure loads are shown in Figures 3a and b (device #3). The deformation could be dynamically controlled by adjusting the contact force set point (Figure 3a). The transfer curves exhibit a strong dependence on the applied pressure. Specifically, the high current on/off ratio (defined as the carrier density/current at the charge neutrality point) pronouncedly increases (Figure 3b). The anomalous transport behavior in Figure 3b can be understood by the competition between the field effect and piezoelectric effect. On one hand, as the positive gate voltage increases, electrons are accumulated on graphene due to the field effect. On the other hand, the applied gate voltage bends graphene through the electrostatic force, resulting in piezoelectric charges. The negligible bending at the initial stage does not influence the total carrier density, which contributes a normal ambipolar transport behavior around the charge neutrality point. However, with large gate voltages, the piezoelectric charges dominate the channel sheet carrier density, creating a decreasing carrier density. As a consequence, the sheet resistance decreases again.

The aforementioned results are absent in control samples made of fully supported graphene, suggesting that the deformation of suspended graphene membrane is the dominant factor that alters the electronic property of graphene (Supplementary Information). The exact origin of the increased resistance contrast is unknown at the current stage. Most likely, a small electrical bandgap (estimated as ~90 meV from the I_{ds}–V_g curves) is opened by the strain field. In contrast to measurements performed on a suspended graphene strip, where the strain direction is at a random angle with the zigzag edge,[31,32] in this NEMS platform, there will always be a radial strain exactly in parallel with the zigzag edge, giving rise to an observable electronic bandgap.

Elucidation of the band-piezoelectric effect

The band-piezoelectric effect can be explained by considering a bandgap opening—the work function mismatch between the bent and supported graphene results in band bending and thus drives charges to separate and accumulate in the space charge region. This process gives rise to polarization across the suspended/supported graphene boundary.

The 2D band-piezoelectric effect arises from the pressure-modified band structure, which highlights the unique property of strain-engineered 2D materials. The band piezoelectricity obtained in conductive graphene is distinctly different from all the traditional piezoelectric effects in two ways. First, a charge transfer process is responsible for the formation of macroscopic dipoles. This process is clearly different from the bulk piezoelectric effect, which is due to the occurrence of electric dipole moments in ions or molecules. Second, the piezoelectric effect typically occurs in insulators because conductive metallic materials have a very short screening length, which weakens the polarization. Here piezoelectricity in semi-metallic

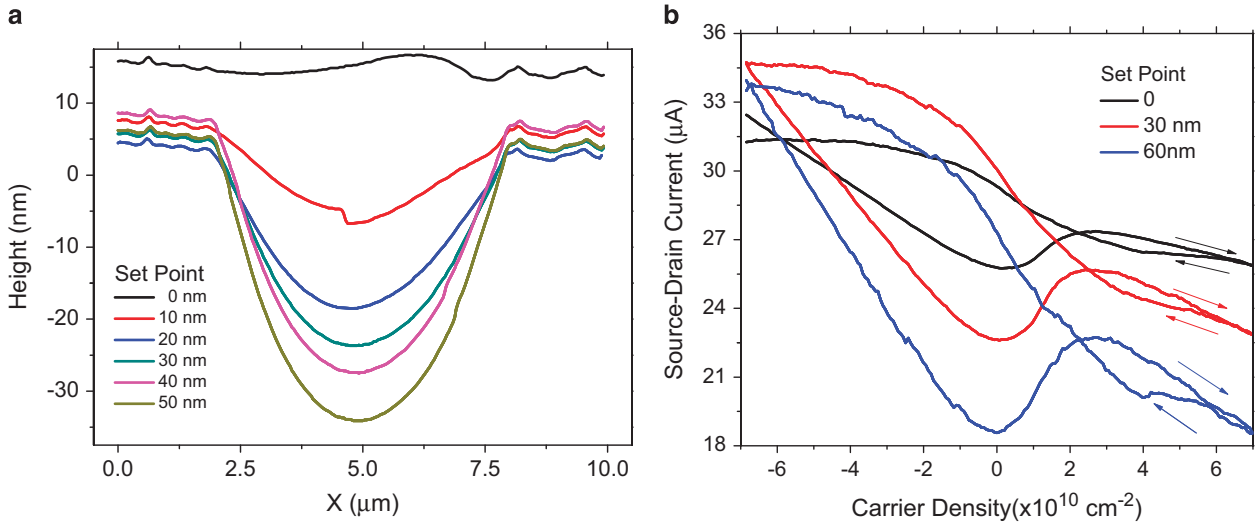

Figure 3 *In situ* transport results of a graphene field-effect transistor based on the deformed suspended graphene membrane. (**a**) Mechanical deformation of the suspended membrane under different contact force set points. (**b**) *In situ* transfer curve (I_{ds} versus V_{gs}) of the suspended graphene membrane under different mechanical loads. The drain-source voltage V_{ds} in these measurements is 50 mV.

graphene is reported, which is due to the low-carrier density in the suspended graphene, yielding a very long screening length and ensuring an observable voltage drop along the device.

Piezoelectric coefficient

Benefitting from its ultrathin and easily bendable structure, the graphene membrane presents an ultrahigh direct piezoelectric coefficient (~37 nC N^{-1}, approximately two orders of magnitude higher than traditional piezoelectric materials and functional graphene[16–17]), although the converse piezoelectric coefficient is small (~12.5 μm V^{-1}) due to graphene's semi-metallic property and large quantum capacitance.

Here we define the piezoelectric coefficients according to the constitutive relations

$$\begin{bmatrix} D \\ \varepsilon \end{bmatrix} = \begin{bmatrix} e & c^{d} \\ c^{c} & s \end{bmatrix} \begin{bmatrix} E \\ \sigma \end{bmatrix}$$

where D, E, ε and σ are the polarized electric displacement vector, the applied electric field vector, the produced stress tensor and the applied strain tensor, respectively. In addition, e, s c^{c} and c^{d} are the dielectric tensor, the elastic compliance tensor, the converse piezoelectric coefficient and the direct piezoelectric coefficient, respectively. To evaluate the piezoelectric material, we consider two piezoelectric coefficients, which are defined as follows:

c^{c}: the strain per unit electric field at constant stress

c^{d}: the electric displacement per unit stress at constant electric field.

Typically, in 2D materials, these two coefficients are 2×2 tensors. In this device configuration, the radial response dominates the experimental results. Therefore, the radial elements could be estimated directly from the definition.

The direct piezoelectric coefficient is estimated for an AFM-pressed nanogenerator experiment. The set point was held at 80 nm, resulting in an ~240 nN pressure force (calculated from the product of the set point and the tip spring constant). The polarized electric displacement is estimated as 6.3×10^{-3} C m^{-2} by multiplying the band bending across the membrane (90 meV for 30 nm of membrane bending) by the quantum capacitance of the suspended graphene (7 μm cm^{-2}). The macroscopic stress is calculated by multiplying the average of the simulated FEM strain in the whole membrane by the Young's modulus (as shown in Figure 1e), resulting in a value of 1.7×10^{5} Pa. From the constitutive law, the direct piezoelectric constant can be calculated as ~37 nC N^{-1}.

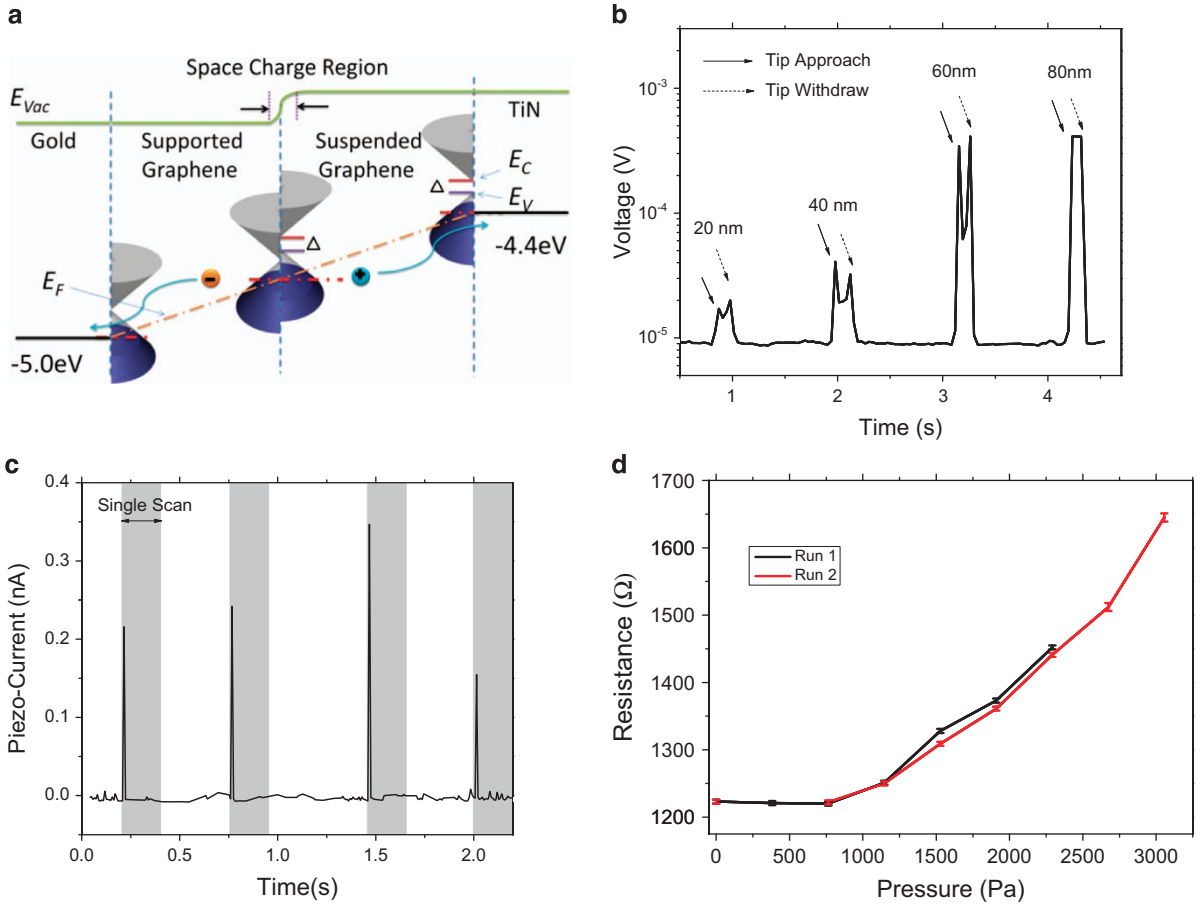

Figure 4 Application of two-dimensional piezoelectric graphene NEMS for energy harvesting and sensing. (**a**) Schematic band structure of the open circuit of the piezoelectric nanogenerator under applied mechanical load. The local Fermi level is marked by a red dashed dot line at the interfaces. The hypothesized bandgap location in the suspended graphene is marked by 'Δ'. (**b**) Output voltage of the graphene membrane-based NEMS nanogenerator under different mechanical loads. The times at which the AFM tip approaches and withdraws from the graphene membrane is marked by solid and dashed arrows, respectively. (**c**) Short circuit current of the suspended graphene membrane nanogenerator. The shaded area marks the time during which the AFM scanning occurs. (**d**) Two terminal resistance of the piezoresistive pressure sensor versus mechanical load. The error bar represents the s.d. AFM, atomic force microscope; NEMS, nanoelectromechanical systems.

Devices utilizing the band-piezoelectronic effect

On the basis of this new type of band-piezoelectric effect, a piezoelectric nanogenerator and a piezoresistive pressure sensor within a graphene NEMS platform have been demonstrated.

A nanogenerator can be designed based on the novel 2D piezoelectric effect. The deformation caused by an AFM tip results in charge separation due to the modified band structure of the bent membrane. Hence, the separated charges can accumulate on external electrodes with proper work functions and produce an output voltage. This process can be depicted by the band diagram of the piezoelectric nanogenerator that is schematically shown in Figure 4a. Note that in the 2D configuration the graphene membrane is always in tensile strain and has an accumulation of positive charges. Therefore, the physical principle for generation of piezoelectric energy in our device is different from, for example, the generation of piezoelectric energy from 1D ZnO nanowires, where the output voltage is determined by the coupling of piezoelectric effect and the semiconducting properties of ZnO.[9]

In the experimental setup, the electronic signal across a large resistive load between the gold cathode and conductive AFM tip (which serves as the anode) was monitored in real time. During the entire measurement, no external bias was applied. As the AFM tip bent the graphene membrane, forward output voltages were detected, as demonstrated in Figure 4b (device #1). The efficiency of the maximum electric power transferred from mechanical energy is estimated as 2.2%. In addition, a two-terminal piezoresistive pressure sensor was fabricated based on the deformation-modified band structure. Replacing the voltmeter by an ammeter, the output current characteristics were revealed, as shown in Figure 4c. Note that there are two factors that limited the measured short circuit current in this device. First, as discussed above, in contrast to conventional semiconductor piezoelectricity, there is no Schottky barrier in this device due to the semi-metallic nature of intrinsic graphene. Second, to maximize the open circuit voltage, an 'inverted' electrode configuration was used, that is, the cathode is a high work function metal, while the anode is a low work function material. Thus, the internal resistance of our nanogenerator is extremely low. Actually, as shown in Figure 4c, the output current quickly decreases after the tip touches the graphene membrane.

As shown in Figure 4d, a reproducible resistance change is observed in response to the applied pressure in the regime where the membrane is not overstressed (device #3). Owing to the one-atom thickness of the layer of graphene, which intuitively leads graphene to be very amendable to external strain, the pressure sensor naturally exhibits a high sensitivity of $\sim 0.2\,\mathrm{kPa}^{-1}$, with a compact footprint.

In conclusion, an unprecedented band-piezoelectric effect on a biaxial-strained suspended graphene NEMS platform was observed. The piezoelectric and piezoresistive effects are attributed to the strain-field-modified band structures. As a result of its ultrathin structure, the graphene NEMS device exhibits an extremely high piezoelectric coefficient up to several $\mathrm{nC\,N}^{-1}$, which is approximately two orders of magnitude higher than that of bulk piezoelectric materials. Unlike piezoelectricity or flexoelectricity, in which the polarization is traced down to the molecular scale, the band-piezoelectric dipoles result from a macroscopic charge accumulation. The applied biaxial strain was observed to shift the work function as well as modify the band structure of the suspended graphene. This effect drives charges with opposite polarities separately in response to the band misalignment through the deformation boundaries. A strain-opened transport bandgap was also hypothesized to explain the observed behavior. On the basis of this NEMS platform, a piezoelectric nanogenerator and a resistive pressure sensor was also fabricated with an energy efficiency of 2.2% and a sensitivity of $0.2\,\mathrm{kPa}^{-1}$. These findings not only open an avenue for novel 2D electromechanical coupling and graphene strain engineering, but also pave the way for sensing, actuating and energy harvesting using graphene NEMS devices.

CONFLICT OF INTEREST

The authors declare no conflict of interest.

ACKNOWLEDGEMENTS

This work was supported by the National Natural Science Foundation of China (61434001, 61025021, 61020106006), the National Key Project of Science and Technology (2011ZX02403-002), the Special Fund for Agro-scientific Research in the Public Interest (201303107), and the Hong Kong RGC GRF grant (4179/10E and N_CUHK405/12). We are thankful for receiving support through the State Key Laboratory of Automotive Safety and Energy, Tsinghua University. HT is additionally supported by the Ministry of Education Scholarship of China. MAM is additionally supported by the postdoctoral fellowship (PDF) program of the Natural Sciences and Engineering Research Council (NSERC) of Canada.

1 Geim, A. K. & Novoselov, K. S. The rise of graphene. *Nat. Mater.* **6**, 183–191 (2007).
2 Bunch, J. S., van der Zande, A. M., Verbridge, S. S., Frank, I. W., Tanenbaum, D. M., Parpia, J. M., Craighead, H. G. & McEuen, P. L. Electromechanical resonators from graphene sheets. *Science* **315**, 490–493 (2007).
3 Lee, C., Wei, X., Kysar, J. W. & Hone, J. Measurement of the elastic properties and intrinsic strength of monolayer graphene. *Science* **321**, 385–388 (2008).
4 Lee, G.-H., Cooper, R. C., An, S. J., Lee, S., van der Zande, A., Petrone, N., Hammerberg, A. G., Lee, C., Crawford, B., Oliver, W., Kysar, J. W. & Hone, J. High-strength chemical-vapor–deposited graphene and grain boundaries. *Science* **340**, 1073–1076 (2013).
5 Chen, C., Rosenblatt, S., Bolotin, K. I., Kalb, W., Kim, P., Kymissis, I., Stormer, H. L., Heinz, T. F. & Hone, J. Performance of monolayer graphene nanomechanical resonators with electrical readout. *Nat. Nanotechnol.* **4**, 861–867 (2009).
6 Park, S., An, J., Suk, J. W. & Ruoff, R. S. Graphene-based actuators. *Small* **6**, 210–212 (2010).
7 Tian, H., Ren, T. L., Xie, D., Wang, Y. F., Zhou, C. J., Feng, T. T., Fu, D., Yang, Y., Peng, P. G., Wang, L. G. & Liu, L. T. Graphene-on-paper sound source devices. *ACS Nano* **5**, 4878–4885 (2011).
8 Smith, A. D., Niklaus, F., Paussa, A., Vaziri, S., Fischer, A. C., Sterner, M., Forsberg, F., Delin, A., Esseni, D., Palestri, P., Östling, M. & Lemme, M. C. Electromechanical piezoresistive sensing in suspended graphene membranes. *Nano Lett.* **13**, 3237–3242 (2013).
9 Wang, Z. L. & Song, J. Piezoelectric nanogenerators based on zinc oxide nanowire arrays. *Science* **312**, 242–246 (2006).
10 Wang, X., Summers, C. J. & Wang, Z. L. Large-scale hexagonal-patterned growth of aligned ZnO nanorods for nano-optoelectronics and nanosensor arrays. *Nano Lett.* **4**, 423–426 (2004).
11 Wang, X., Song, J., Liu, J. & Wang, Z. L. Direct-current nanogenerator driven by ultrasonic waves. *Science* **316**, 102–105 (2007).
12 Qi, Y., Jafferis, N. T., Lyons, K. Jr, Lee, C. M., Ahmad, H. & McAlpine, M. C. Piezoelectric ribbons printed onto rubber for flexible energy conversion. *Nano Lett.* **10**, 524–528 (2010).
13 Mengüç, Y., Yang, S. Y., Kim, S., Rogers, J. A. & Sitti, M. Gecko-inspired controllable adhesive structures applied to micromanipulation. *Adv. Funct. Mater.* **22**, 1246–1254 (2012).
14 Persano, L., Dagdeviren, C., Su, Y., Zhang, Y., Girardo, S., Pisignano, D., Huang, Y. & Rogers, J. A. High performance piezoelectric devices based on aligned arrays of nanofibers of poly(vinylidenefluoride-co-trifluoroethylene). *Nat. Commun.* **4**, 1633 (2013).
15 Ong, M. T. & Reed, E. J. Engineered piezoelectricity in graphene. *ACS Nano* **6**, 1387–1394 (2011).
16 Zelisko, M., Hanlumyuang, Y., Yang, S., Liu, Y., Lei, C., Li, J., Ajayan, P. M. & Sharma, P. Anomalous piezoelectricity in two-dimensional graphene nitride nanosheets. *Nat. Commun.* **5**, 4284 (2014).
17 Chandratre, S. & Sharma, P. Coaxing graphene to be piezoelectric. *Appl. Phys. Lett.* **100**, 023114 (2012).
18 Catalan, G., Lubk, A., Vlooswijk, A. H., Snoeck, E., Magen, C., Janssens, A., Rispens, G., Rijnders, G., Blank, D. H. & Noheda, B. Flexoelectric rotation of polarization in ferroelectric thin films. *Nat. Mater.* **10**, 963–967 (2011).
19 Lu, H., Bark, C. W., Esque de los Ojos, D., Alcala, J., Eom, C. B., Catalan, G. & Gruverman, A. Mechanical writing of ferroelectric polarization. *Science* **336**, 59–61 (2012).

20 Pereira, V. M. & Neto, A. H. C. Strain engineering of graphene's electronic structure. *Phys. Rev. Lett.* **103**, 046801 (2009).
21 Guinea, F., Katsnelson, M. I. & Geim, A. K. Energy gaps and a zero-field quantum Hall effect in graphene by strain engineering. *Nat. Phys.* **6**, 30–33 (2010).
22 Zhou, S. Y., Gweon, G. H., Fedorov, A. V., First, P. N., de Heer, W. A., Lee, D. H., Guinea, F., Castro Neto, A. H. & Lanzara, A. Substrate-induced bandgap opening in epitaxial graphene. *Nat. Mater.* **6**, 770–775 (2007).
23 Ni, Z. H., Yu, T., Lu, Y. H., Wang, Y. Y., Feng, Y. P. & Shen, Z. X. Uniaxial strain on graphene: Raman spectroscopy study and band-gap opening. *ACS Nano* **2**, 2301–2305 (2008).
24 Lee, J.-U., Yoon, D. & Cheong, H. Estimation of Young's modulus of graphene by Raman spectroscopy. *Nano Lett.* **12**, 4444–4448 (2012).
25 Klimov, N. N., Jung, S., Zhu, S., Li, T., Wright, C. A., Solares, S. D., Newell, D. B., Zhitenev, N. B. & Stroscio, J. A. Electromechanical properties of graphene drumheads. *Science* **336**, 1557–1561 (2012).
26 Hicks, J., Tejeda, A., Taleb-Ibrahimi, A., Nevius, M. S., Wang, F., Shepperd, K., Palmer, J., Bertran, F., Le Fèvre, P., Kunc, J., de Heer, W. A., Berger, C. & Conrad, E. H. A wide-bandgap metal-semiconductor-metal nanostructure made entirely from graphene. *Nat. Phys.* **9**, 49–54 (2013).
27 Novoselov, K. S., Geim, A. K., Morozov, S. V., Jiang, D., Zhang, Y., Dubonos, S. V., Grigorieva, I. V. & Firsov, A. A. Electric field effect in atomically thin carbon films. *Science* **306**, 666–669 (2004).
28 Bao, W., Myhro, K., Zhao, Z., Chen, Z., Jang, W., Jing, L., Miao, F., Zhang, H., Dames, C. & Lau, C. N. In situ observation of electrostatic and thermal manipulation of suspended graphene membranes. *Nano Lett.* **12**, 5470–5474 (2012).
29 Wang, X. M., Xu, J.-B., Wang, C. L., Xie, W. G. & Du, J. High performance graphene devices on SiO_2/Si substrate modified by highly-ordered self-assembled monolayers. *Adv. Mater.* **23**, 2464–2468 (2011).
30 Bao, W., Miao, F., Chen, Z., Zhang, H., Jang, W., Dames, C. & Lau, C. N. Controlled ripple texturing of suspended graphene and ultrathin graphite membranes. *Nat. Nanotechnol.* **4**, 562–566 (2009).
31 Huang, M., Pascal, T. A., Kim, H., Goddard, W. A. & Greer, J. R. Electronic–mechanical coupling in graphene from in situ nanoindentation experiments and multiscale atomistic simulations. *Nano Lett.* **11**, 1241–1246 (2011).
32 Choi, S.-M., Jhi, S.-H. & Son, Y.-W. Effects of strain on electronic properties of graphene. *Phys. Rev. B* **81**, 081407 (2010).

Supplementary Information accompanies the paper on the NPG Asia Materials website (http://www.nature.com/am)